Johann Radon Institute for
Computational and Applied Mathematics
Austrian Academy of Sciences (ÖAW)

On detection and visibility of a complex obstacle using multipoles sources from far field data

J. Liu, M. Sini

RICAM-Report 2008-14

ON DETECTION AND VISIBILITY OF A COMPLEX OBSTACLE USING MULTIPOLES SOURCES FROM FAR FIELD DATA

J.J. LIU M. SINI
DEPARTMENT OF MATHEMATICS, SOUTHEAST UNIVERSITY
NANJING, 210096, P.R.CHINA. EMAIL: JJLIU@SEU.EDU.CN
JOHANN RADON INSTITUTE FOR COMPUTATIONAL AND APPLIED MATHEMATICS
AUSTRIAN ACADEMY OF SCIENCE
LINZ, A-4040, AUSTRIA. EMAIL: MOURAD.SINI@OEAW.AC.AT

Abstract. We deal with the acoustic inverse scattering problem for detecting an obstacle with mixed boundary conditions from the far field map. We show how the geometric properties and the material parameter distributed on the surface are involved in the obstacle reconstruction numerically. The main advance of this research on our recently work (SIAM J. Applied Math, 67(4), 2007) is the higher-order asymptotic expansion of the indicator function and the introduction of complex valued surface impedance, which makes the reconstruction more (or less) accurate depending on how we choose this surface impedance. Precisely, using the relation between the surface impedance and the obstacle curvature contained in the higher-order expansion of the indicators, we reveal how the obstacle curvature and the surface impedance on the coated part influence the blowing-up behavior. Using this theoretical result, we can specify the complex surface impedance in terms of the obstacle curvature to make the obstacle more (or less) visible. By establishing the property of the minimum norm solution for approximating the singular sources, efficient realizations for approximating the multipoles by Herglotz wave function and therefore the implementations of the probing methods are developed with an error estimate. Such an estimate gives a thorough explanation on the reasons why these probing methods can reach only finite accuracy of reconstruction. We finally show extensive numerical tests explaining how and to what extent the coupling relation between the curvature and the surface impedance changes the visibility of the obstacles.

Key words. Inverse scattering, far field, impedance boundary, regularization, minimum norm solution, numerics.

AMS subject classifications. 35P25, 35R30, 45Q05, 78A45.

1. Introduction.

The inverse scattering problems by complex impenetrable obstacles have received much attention in recent years due to their potential applications, see for instance [7, 10, 30] for different analytical methods and [14] and [4] for practical motivations in military coatings and marine acoustics. By a complex obstacle, we mean an obstacle whose boundary is characterized by its geometry as well as the acoustic properties modeled by appropriate material distributed along a part or the whole surface. Regarding the size, we distinguish three types of obstacles:

- The point-like obstacles whose sizes are much smaller than the array resolution, see [11, 13, 18, 29, 31].
- The small obstacles whose sizes are smaller than, but comparable to the array resolution, see [1, 2, 3, 12, 30].
- The extended obstacles whose sizes are larger than the array resolution, see [7, 10, 17].

In this work, we are interested in the boundary reconstruction for the third class of obstacles. Our inversion input data are far field patterns produced by many incident plane waves, with the goal of reconstructing the complex extended obstacle from these data. Instead of considering a full 3-dimensional electromagnetism model, we restrict ourself to the 2-dimensional Helmholtz model, which is well known to be an approximate model in case if the obstacle is of a cylinder form in $\mathbb{R}^3$, see [7].

This problem has a quite long history, see for instance [5, 6, 7, 8, 10, 17, 20, 27, 28, 30]. There are several methods proposed to solve this problem. We are inter-

ested by the non-iterative ones, like the linear sampling method [9], the factorization method [19], the MUSIC algorithm [11], the probe method [16] and the singular sources method [26]. All these methods build indicator functions depending on a parameter given by the source points. The reconstruction of the shape of the obstacle, by these methods, is based on the drastic behavior of the corresponding indicator functions when the source point approaches the interface of the obstacle. To our opinion, the way how these indicator functions blowup is the crucial point to understand the numerical performance of these theoretically elegant reconstruction methods.

In a recent work [23, 24], we started such studies by taking as pilot the probing method (as the probe and the singular sources methods, see [15, 25]). Precisely, using multipoles of order two as point sources, we derived in [23] the asymptotic expansion of the indicator functions with respect to the source point. We found out that the first order term in the expansion involves the unit normals of the interface, while the second (lower) order term involves a combination of the surface curvature and the imaginary part of the surface impedance. This behavior may explain why, for example, reconstructing convex objects is easier and more accurate than reconstructing non-convex ones. In addition, this analysis also suggests some possible ways for making the reconstruction more (or less) accurate by using the artificially introduced *complex* surface impedance. We think that these new observations may have some potential applications for instance in military coatings, see [14], and marine acoustics, see [4].

Let D be a bounded domain of $\mathbb{R}^2$ such that $\mathbb{R}^2 \setminus \overline{D}$ is connected. We assume that its boundary ∂D is of class $C^{2,1}$ with the decomposition $\partial D = \overline{\partial D_I} \cup \overline{\partial D_D}$, $\partial D_I \cap \partial D_D = \emptyset$, where ∂D_D and ∂D_I are open curves in ∂D.

The propagation of time-harmonic acoustic wave in homogeneous media outside a cylinder in $\mathbb{R}^3$ can be modeled by 2-dimensional Helmholtz equation with some boundary condition. For given incident plane wave $u^i(x) = e^{i\kappa d\cdot x}$ and a complex impenetrable obstacle $D \subset \mathbb{R}^2$ with $C^{2,1}$-smooth boundary, the total wave $u(x) = u^i(x) + u^s(x)$ is governed by the following exterior problem

$$\begin{cases} \Delta u + \kappa^2 u = 0 & \text{in } \mathbb{R}^2 \setminus \overline{D}, \\ u = 0 & \text{on } \partial D_D, \\ \frac{\partial u}{\partial \nu} + i\kappa\sigma u = 0 & \text{on } \partial D_I, \end{cases} \tag{1.1}$$

where $\nu(x)$ is the outward normal direction of ∂D. We assume that the surface impedance $\sigma(x) := \sigma^r(x) + i\sigma^i(x)$ is a complex-valued Lipschitz continuous function, and its real part $\sigma^r(x)$ has a uniform lower bound $\sigma_0^r > 0$ on ∂D_I. The part ∂D_I is referred to by the coated part of ∂D and ∂D_D is the non-coated part. To the best of our knowledge, the researches of inverse scattering problems up to now always consider the case $\sigma^i(x) \equiv 0$. We will see that the introduction of nonzero $\sigma^i(x)$ has great numerical influence on the shape reconstruction of an obstacle.

On the other hand, it is also well-known that the scattered field u^s satisfies the Sommerfeld radiation condition

$$\lim_{r\to\infty} \sqrt{r}\left(\frac{\partial u^s}{\partial r} - i\kappa u^s\right) = 0 \tag{1.2}$$

with $r = |x|$ and has the following asymptotic expansion

$$u^s(x,d) = \frac{e^{i\kappa|x|}}{\sqrt{|x|}}\left(u^\infty(\hat{x},d) + O\left(\frac{1}{|x|}\right)\right), \quad \hat{x} = \frac{x}{|x|} \in \mathbb{S} \tag{1.3}$$

as $|x| \to \infty$, where $\mathbb{S}$ is the unite cycle in $\mathbb{R}^2$. $u^\infty(\hat{x}, d)$ is called as the far-field pattern of scattered wave $u^s(x, d)$.

The mixed problem (1.1)-(1.2) is well posed. More generally, for $f \in H^{\frac{1}{2}}(\partial D_D)$ and $h \in H^{-\frac{1}{2}}(\partial D_I)$, there exists a unique solution of the mixed problem

$$\begin{cases} (\Delta + \kappa^2)u = 0, & \text{in } \mathbb{R}^2 \setminus \overline{D}, \\ u = f & \text{on } \partial D_D, \\ \frac{\partial u}{\partial \nu} + i\kappa\sigma u = h, & \text{on } \partial D_I, \\ \frac{\partial u}{\partial r} - i\kappa u = o(\frac{1}{\sqrt{r}}), & r \to \infty \end{cases} \tag{1.4}$$

and the solution satisfies

$$\|u\|_{H^1(\Omega_R \cap (\mathbb{R}^2 \setminus \overline{D}))} \leq C_R(\|f\|_{H^{1/2}(\partial D_D)} + \|h\|_{H^{-1/2}(\partial D_I)}), \tag{1.5}$$

where Ω_R is a disk of radius R and C_R is positive constant, see [7] for more details.

For the above scattering problem by a complex obstacle, the inverse scattering problem is stated as following.

Given $u^\infty(\cdot, \cdot)$ on $\mathbb{S} \times \mathbb{S}$ for the scattering problem (1.1)-(1.3), we need to

- Reconstruct the shape of the obstacle D;
- Reconstruct some geometry properties of ∂D such as normal directions and the curvature;
- Distinguish the coated part ∂D_I from the non coated part ∂D_D;
- Reconstruct the complex surface impedance $\sigma(x)$ on ∂D_I, including the real and the imaginary parts.

Remark 1.1. *Theoretically speaking, both normal direction of ∂D and its curvature are completely determined once ∂D is known. However, since ∂D is reconstructed approximately in inverse scattering problem, the determination of the obstacle curvature and the normal directions from the approximate ∂D is ill-posed. From the numerical point of view, we need to detect these two geometric information from the far-field data directly.*

The aim of this paper is to propose an efficient realization of this new inversion scheme of the probe method using the higher order expansions of its indicator function as proposed in [23] and to analyze the reconstruction accuracy mathematically. We address the following three points:

- How to construct the indicator functions numerically and efficiently.
- Numerical implementations to show reconstructions of complex obstacles. Since such a detection method (and actually any of the previously mentioned probing or sampling methods) uses the limit behavior of some indicator functions to probe the obstacle boundary as well as the surface impedance, the numerical performance of this theoretically elegant method is of great importance for its practical application. That is, we need to understand to what extent this method can approximate the unknown ingredients numerically and what is the amount of computation. More precisely, this method uses some needle to detect the boundary points from all the directions. Therefore we need an efficient realization of this method.
- Numerical implementations to show how we can increase or decrease the visibility of an obstacle by balancing the surface impedance and the obstacle curvature.

As we already mentioned, in our previous paper [23] we showed that the combined effect of surface impedance and the concavity of the obstacle makes the scattering process much more complicated. However, by using explicit combinations of the surface impedance and the curvature, we show that the visibility of the obstacle can be controlled . The key idea is to change the blowing-up behavior of indicator functions by adjusting the relation of surface impedance and the obstacle curvature.

This paper is organized as follows. In section 2, we give the expansion results for all unknowns presented in [23] and rewrite them in an equivalently way. Such an equivalent form is important for our numerical realization. Then in section 3, we discuss the efficient approximation for multiploes on the boundary of the approximate domain by establishing the property of minimum norm solution. The error estimate on the singular source approximation as well as the choice of dimension of approximate function space, which takes an important role in the construction of indicator function, is given in section 4. Finally, we present some numerical results in section 5 .

2. Presentation of the asymptotic results and equivalent forms. Due to the superposition principle, the scattered field associated with the Herglotz incident field $v_g^i := v_g(x)$ defined by

$$v_g(x) := \int_{\mathbb{S}} e^{i\kappa x\cdot d} g(d)\, ds(d), \quad x \in \mathbb{R}^2 \tag{2.1}$$

with $g \in L^2(\mathbb{S})$ is given by

$$v_g^s(x) := \int_{\mathbb{S}} u^s(x,d) g(d)\, ds(d), \quad x \in \mathbb{R}^2 \setminus \overline{D}, \tag{2.2}$$

and its far field is

$$v_g^\infty(\hat{x}) := \int_{S^1} u^\infty(\hat{x},d) g(d)\, ds(d), \quad \hat{x} \in \mathbb{S}. \tag{2.3}$$

Denote by $\Phi(x,z) = \frac{i}{4} H_0^{(1)}(\kappa|x-z|)$ the fundamental solution for the Helmholtz equation in $\mathbb{R}^2$. Assume that $\overline{D} \subset\subset \Omega$ for some known Ω with smooth boundary. For $a \in \Omega \setminus D$, denote by $\{z_p\} \subset \Omega \setminus \overline{D}$ a sequence tending to a. For any z_p, set D_a^p a C^2-regular domain such that $\overline{D} \subset D_a^p$ (resp. $\overline{\partial D} \subset D_a^p$) with $z_q \in \Omega \setminus \overline{D_a^p}$ for every $q = 1, 2, \cdots, p$ and that the Dirichlet interior problem on D_a^p for the Helmholtz equation is uniquely solvable. In this case, the Herglotz wave operator $\mathbb{H}$ from $L^2(\mathbb{S})$ to $L^2(\partial D_a^p)$ defined by

$$\mathbb{H}[g](x) := v_g(x) = \int_{\mathbb{S}} e^{i\kappa x\cdot d} g(d)\, ds(d) \tag{2.4}$$

is injective, compact with dense range, see [10]. Now we consider the sequence of point sources: pole $\Phi(\cdot, z_p)$, dipoles $\frac{\partial}{\partial x_j}\Phi(\cdot,z)$ and multipoles of order two $\frac{\partial}{\partial x_j}\frac{\partial}{\partial x_2}\Phi(\cdot,z)$ for $j = 1, 2$. For every p fixed, we construct three density sequences $\{g_n^p\}$, $\{f_m^{j,p}\}$ and $\{h_k^{j,p}\}$ in $L^2(\mathbb{S})$ with $j = 1, 2$, by the Tikhonov regularization such that

$$\|v_{g_n^p} - \Phi(\cdot, z_p)\|_{L^2(\partial D_a^p)} \to 0, \quad n \to \infty, \tag{2.5}$$

$$\|v_{f_m^{j,p}} - \frac{\partial}{\partial x_j}\Phi(\cdot, z_p)\|_{L^2(\partial D_a^p)} \to 0, \quad m \to \infty, \tag{2.6}$$

$$\|v_{h_k^{j,p}} - \frac{\partial}{\partial x_j}\frac{\partial}{\partial x_2}\Phi(\cdot, z_p)\|_{L^2(\partial D_a^p)} \to 0, \quad k \to \infty. \tag{2.7}$$

Using these three density sequences, we construct the following three indicators

$$I^0(z_p) := \frac{1}{\gamma_2} \lim_{m\to\infty} \lim_{n\to\infty} \int_{\mathbb{S}}\int_{\mathbb{S}} u^\infty(-\hat{x}, d)\ g_m^p(d)\ g_n^p(\hat{x})\ ds(\hat{x})ds(d), \tag{2.8}$$

$$I_j^1(z_p) := \frac{1}{\gamma_2} \lim_{m\to\infty} \lim_{n\to\infty} \int_{\mathbb{S}}\int_{\mathbb{S}} u^\infty(-\hat{x}, d)\ f_m^{j,p}(d)\ g_n^p(\hat{x})\ ds(\hat{x})ds(d), \tag{2.9}$$

$$I_j^2(z_p) := \frac{1}{\gamma_2} \lim_{m\to\infty} \lim_{n\to\infty} \int_{\mathbb{S}}\int_{\mathbb{S}} u^\infty(-\hat{x}, d)\ h_m^{j,p}(d)\ g_n^p(\hat{x})\ ds(\hat{x})ds(d), \tag{2.10}$$

where $\gamma_2 = e^{i\pi/4}/\sqrt{8\pi\kappa}$.

For the points $a \in \partial D$, we choose the sequence $\{z_p\}_{p\in\mathbb{N}}$ included in $C_{a,\theta}$, where $C_{a,\theta}$ is a cone with center a, angle $\theta \in [0, \frac{\pi}{2})$ and axis $\nu(a)$. The following theoretical result is given in [23].

THEOREM 2.1. *Assume that the boundary ∂D is of class $C^{2,1}$ and $\sigma = \sigma^r + i\sigma^i$ defined in ∂D_I is the complex surface impedance. Then the above three indicators have the following asymptotic formulas:*

I. For pole $\Phi(x, z)$ as source, it follows that

$$\text{Re } I^0(z_p) = \begin{cases} -\frac{1}{4\pi}\ln|(z_p - a)\cdot\nu(a)| + O(1), & a \in \partial D_I, \\ +\frac{1}{4\pi}\ln|(z_p - a)\cdot\nu(a)| + O(1), & a \in \partial D_D. \end{cases} \tag{2.11}$$

$$\text{Im} I^0(z_p) = O(1), \quad a \in \partial D. \tag{2.12}$$

II. Using dipoles $\frac{\partial}{\partial x_j}\Phi(x, z)$ with $j = 1, 2$ as sources, it follows that

$$\text{Re } I_j^1(z_p) = \begin{cases} \frac{\nu_j(a)}{4\pi|(z_p-a)\cdot\nu(a)|} + \frac{\nu_j(a)\kappa\sigma^i(a)}{\pi}\ln|(z_p - a)\cdot\nu(a)| + O(1), & a \in \partial D_I, \\ \frac{-\nu_j(a)}{4\pi|(z_p-a)\cdot\nu(a)|} + O(1), & a \in \partial D_D. \end{cases} \tag{2.13}$$

$$\text{Im } I_j^1(z_p) = \begin{cases} -\frac{\nu_j(a)\kappa\sigma^r(a)}{\pi}\ln|(z_p - a)\cdot\nu(a)| + O(1), & a \in \partial D_I, \\ O(1), \quad a \in \partial D_D. \end{cases} \tag{2.14}$$

III. Using multipoles of order two $\frac{\partial}{\partial x_j}\frac{\partial}{\partial x_2}\Phi(x, z)$ with $j = 1, 2$, it follows that

$$\text{Re } I_1^2(z_p) = \begin{cases} \frac{\nu_1(a)\nu_2(a)}{4\pi|(z_p-a)\cdot\nu(a)|^2} + \frac{(2\nu_1(a)\nu_2(a)\kappa\sigma^i(a) + f''(a)(2\nu_1(a)\nu_2(a) + \nu_2(a)^2 - \nu_1^2(a)))}{2\pi|(z_p-a)\cdot\nu(a)|} + \\ O(\ln|(z_p - a)\cdot\nu(a)|), \quad a \in \partial D_I, \\ \frac{-\nu_1(a)\nu_2(a)}{4\pi|(z_p-a)\cdot\nu(a)|^2} + \frac{f''(a)(2\nu(a)_1\nu_2(a) + \nu_2^2(a) - \nu_1^2(a))}{2\pi|(z_p-a)\cdot\nu(a)|} + \\ O(\ln|(z_p - a)\cdot\nu(a)|), \quad a \in \partial D_D. \end{cases} \tag{2.15}$$

$$\text{Re } I_2^2(z_p) = \begin{cases} \frac{\nu_2^2(a) - \nu_1^2(a)}{8\pi|(z_p-a)\cdot\nu(a)|^2} + \frac{(\nu_2^2(a) - \nu_1^2(a))\kappa\sigma^i(a) + f''(a)(\nu_2^2(a) - \nu_1^2(a) - 2\nu_1(a)\nu_2(a))}{2\pi|(z_p-a)\cdot\nu(a)|} + \\ O(\ln|(z_p - a)\cdot\nu(a)|), \quad a \in \partial D_I, \\ \frac{\nu_1^2(a) - \nu_2^2(a)}{8\pi|(z_p-a)\cdot\nu(a)|^2} + \frac{f''(a)(\nu_2^2(a) - \nu_1^2(a) - 2\nu_1(a)\nu_2(a))}{2\pi|(z_p-a)\cdot\nu(a)|} + \\ O(\ln|(z_p - a)\cdot\nu(a)|), \quad a \in \partial D_D. \end{cases} \tag{2.16}$$

and

$$\text{Im } I_1^2(z_p) = \begin{cases} \frac{-\nu_1(a)\nu_2(a)}{\pi|(z_p-a)\cdot\nu(a)|}\kappa\sigma^r + O(\ln|(z_p-a)\cdot\nu(a)|), & a\in\partial D_I, \\ O(\ln|(z_p-a)\cdot\nu(a)|), & a\in\partial D_D. \end{cases} \tag{2.17}$$

$$\text{Im } I_2^2(z_p) = \begin{cases} \frac{\nu_1^2(a)-\nu_2^2(a)}{2\pi|(z_p-a)\cdot\nu(a)|}\kappa\sigma^r + O(\ln|(z_p-a)\cdot\nu(a)|), & a\in\partial D_I, \\ O(\ln|(z_p-a)\cdot\nu(a)|), & a\in\partial D_D. \end{cases} \tag{2.18}$$

These theoretical results will be used for our numerical realization in different but equivalent forms for reconstructing the obstacle. These formulas can be used in the following situations.

1. The obstacles are unknown. In this case, we know nothing about the obstacle shape, boundary type and surface impedance. However, the combination of the above formula make us to detect the obstacle without the knowledge of surface impedance.

- Use (2.11) to detect the boundary shape and the type, that is,

$$\lim_{z_p\to a} \text{Re } I^0(z_p) = \begin{cases} +\infty, & a\in\partial D_I, \\ -\infty, & a\in\partial D_D. \end{cases} \tag{2.19}$$

The other way to detect the location and type of ∂D is

$$\lim_{z_p\to a}\sum_{j=1}^{2}(\text{Re } I_j^1)^2 = \begin{cases} \lim_{z_p\to a}\left[\frac{1}{16\pi^2|(z_p-a)\cdot\nu(a)|^2} + \frac{\kappa\sigma^i\ln|(z_p-a)\cdot\nu(a)|}{2\pi^2|(z_p-a)\cdot\nu(a)|}\right] + \\ \quad O(\frac{1}{4\pi|(z_p-a)\cdot\nu(a)|}) = +\infty,\ a\in\partial D_I, \\ \lim_{z_p\to a}\frac{1}{16\pi^2|(z_p-a)\cdot\nu(a)|^2} + \\ \quad O(\frac{1}{4\pi|(z_p-a)\cdot\nu(a)|}) = +\infty,\ a\in\partial D_D \end{cases} \tag{2.20}$$

$$\lim_{z_p\to a}\sum_{j=1}^{2}(\text{Im } I_j^1)^2 = \begin{cases} \frac{(\kappa\sigma^r)^2}{\pi^2}\lim_{z_p\to a}\ln^2|(z_p-a)\cdot\nu(a)| + \\ \quad O(\ln|(z_p-a)\cdot\nu(a)|) = \infty,\ a\in\partial D_I \\ O(1),\ a\in\partial D_D \end{cases} \tag{2.21}$$

in terms of (2.13) and (2.14). By analyzing these asymptotic behavior, it is suggested to use (2.20) for detecting the shape and to use (2.19) for detecting the type.

- The above formula can only give an approximation to ∂D numerically. Therefore the normal derivative $\nu(a)$ may be of large error using approximate ∂D from the formula (2.19) or (2.20). However, using the dipoles formulas (2.13), the normal direction can be determined from

$$\nu(a) = (\pm t\sqrt{\frac{1}{1+t^2}}, \pm\sqrt{\frac{1}{1+t^2}}) \text{ where } t := \lim_{z_p\to a}\frac{\text{Re } I_1^1(z_p)}{\text{Re } I_2^1(z_p)} = \frac{\nu_1(a)}{\nu_2(a)} \tag{2.22}$$

almost everywhere, except for some points satisfying $\nu_2(a)=0$. In case that t is quite large which means $\nu_2(a)\approx 0$, the normal direction at a can be computed from

$$\nu(a) = (\pm\sqrt{\frac{1}{1+\tilde{t}^2}}, \pm\tilde{t}\sqrt{\frac{1}{1+\tilde{t}^2}}) \text{ where } \tilde{t} := \lim_{z_p\to a}\frac{\text{Re } I_2^1(z_p)}{\text{Re } I_1^1(z_p)} = \frac{\nu_2(a)}{\nu_1(a)} \tag{2.23}$$

Therefore the geometric properties for D are determined. The sign $\pm$ can be fixed by the orientation of ∂D and the rough reconstruction of ∂D. More precisely, for $\nu = (x_2'(t), -x_1'(t))$, the sign of each component can be determined from the tangential direction $\tau := (x_1'(t), x_2'(t))$ of a reasonable approximation of ∂D. That is, a reasonable approximation of ∂D can give us the correct sign of each component of τ.

- Using the multipoles formulas, the curvature is computable from known normal direction of ∂D and surface impedance σ. That is,

$$f''(a) = -\kappa\sigma^i(a) + 2\lim_{z_p\to a}\{\frac{\pi[2\nu_1(a)\nu_2(a)\mathrm{Re}\, I_1^2(z_p) + (\nu_2^2(a)-\nu_1^2(a))\mathrm{Re}\, I_2^2(z_p)]}{|(z_p-a)\cdot\nu(a)|^{-1}} - \frac{1}{8|(z_p-a)\cdot\nu(a)|}\} \text{ for } a\in\partial D_I \tag{2.24}$$

and

$$f''(a) = 2\lim_{z_p\to a}\{\frac{\pi[2\nu_1(a)\nu_2(a)\mathrm{Re}\, I_1^2(z_p) + (\nu_2^2(a)-\nu_1^2(a))\mathrm{Re}\, I_2^2(z_p)]}{|(z_p-a)\cdot\nu(a)|^{-1}} + \frac{1}{8|(z_p-a)\cdot\nu(a)|}\} \text{ for } a\in\partial D_D \tag{2.25}$$

where $\sigma^i(a)$ is computable by using $I_j^1, j=1,2$, as:

$$\sigma^i(a) = \lim_{z_p\to a}\frac{\pi\sum_{j=1}^2\nu_j(a)\mathrm{Re}\, I_j^1(z_p) - \frac{1}{4|(z_p-a)\cdot\nu(a)|}}{\kappa\ln|(z_p-a)\cdot\nu(a)|}, \quad a\in D_I. \tag{2.26}$$

- The geometric shape and type have been determined by the above two steps. Now we can determine the real part of the surface impedance by (2.13). That is,

$$\sigma^r(a) = -\lim_{z_p\to a}\frac{\pi\sum_{j=1}^2\nu_j(a)\mathrm{Im}\, I_j^1(z_p)}{\kappa\ln|(z_p-a)\cdot\nu(a)|}, \quad a\in D_I. \tag{2.27}$$

Using (2.17) and (2.18), we can identify $\sigma^r(x)$ from the other formula:

$$-\frac{2\pi}{\kappa}\lim_{z_p\to a}\frac{2\nu_1(a)\nu_2(a)\mathrm{Im}\, I_1^2(z_p) + (\nu_2^2(a)-\nu_1^2(a))\mathrm{Im}\, I_2^2(z_p)}{|(z_p-a)\cdot\nu(a)|^{-1}} = \sigma^r(a), a\in\partial D_I.$$

The counterpart of this relation is (2.24). That is, (2.24) can also be used to determine $\sigma^i(a)$ for given ∂D.

2. Controlling the visibility of the obstacle. We can make the obstacle more (or less) visible by adjusting the relation between curvature and surface impedance.

- If we know the obstacle shape and wish to make it more visible, then we can choose the surface impedance (the coating coefficient) as

$$\sigma^i(a) \le -\frac{f''(a)}{\kappa} \quad \text{or } \sigma^i(a) \ge -\frac{f''(a)}{\kappa} \text{ for every } a\in\partial D_I \tag{2.28}$$

and take $\partial D_I = \partial D$, i.e. distribute the coating coefficient along all the surface of the obstacle. Indeed, using the formula

$$\begin{aligned} &2\nu_1(a)\nu_2(a)\mathrm{Re}\, I_1^2(z_p) + (\nu_2^2(a)-\nu_1^2(a))\mathrm{Re}\, I_2^2(z_p) \\ &= \frac{1}{8\pi|(z_p-a)\cdot\nu(a)|^2} + \frac{f''(a)+k\sigma^i(a)}{\pi|(z_p-a)\cdot\nu(a)|} + O(\ln|(z_p-a)\cdot\nu(a)|), \end{aligned} \tag{2.29}$$

the condition $f''(a) + \kappa\sigma^i(a) \geq 0$ increases the blow-up of the right-hand side while the condition $f''(a) + \kappa\sigma^i(a) \leq 0$ decreases the blow-up. However, we need to choose $f''(a) + \kappa\sigma^i(a)$ uniform on ∂D. In this case, the obstacle will be seen mostly as a uniform Dirichlet obstacle with a uniform curvature. Indeed, the blowup of the indicator functions $I_j(z)$ are uniform around the obstacle which makes the obstacle uniformly visible from the measurements. So the uniform feature of $f''(a) + \kappa\sigma^i(a)$ is the most important and not the sign. For example, for the case $f''(a) + \kappa\sigma^i(a) = 0$, we have

$$\begin{aligned} &2\nu_1(a)\nu_2(a)\text{Re } I_1^2(z_p) + (\nu_2^2(a) - \nu_1^2(a))\text{Re } I_2^2(z_p) \\ &= \frac{1}{8\pi|(z_p - a)\cdot\nu(a)|^2} + O(\ln|(z_p - a)\cdot\nu(a)|), \quad a \in \partial D. \end{aligned} \tag{2.30}$$

In this case, the obstacle will be seen mostly as a uniform Dirichlet obstacle with zero curvature (i.e. a linear crack).

- If we wish the obstacle less visible, then we can choose σ^i on ∂D_I to be non-uniformly distributed (i.e highly oscillating) so that the blowup of the indicator functions $I_j(z)$ would be less uniform around the obstacle. This perturbs its visibility.

Notice that in our previous paper [22] for mixed boundary condition, we always assume that $\sigma^i \equiv 0$. We have seen in this paper that the introduction of nonzero σ^i have an important effect on the reconstruction of the boundary shape.

3. Construction of density function for the indicator. In this section, we consider how to compute approximation of the point source in ∂D_a^p efficiently, since in detecting the obstacle boundary, the approximated domain ∂D_a^p needs to be chosen for z_p approaching to ∂D along all directions. If we get this approximation always by solving the minimum norm solution in ∂D_a^p, then the amount of computation will be quite large. Notice that the key points in the detection are to find density function g, f, h such that the approximations (2.5)-(2.7) hold. Constructing these three functions by minimum norm solutions is just one possible way, not the only way. Such an observation makes us to compute the singular sources approximation in all approximate domain in an efficient and simple way.

We will show in this section that, if the approximation domain D_a^p is constructed from some fixed reference domain D_0 by rotation and translation, then these three functions can be constructed from the related minimum norm solutions defined in the fixed domain ∂D_0, using a simple function transform depending on the rotation matrix and translation vector. By this technique, the amount of computation for constructing the indicator function will be decreased dramatically.

For given fixed reference domain G_0 with $0 \notin G_0$ and smooth boundary ∂G_0, let G be a domain generated from G_0 by rotation and translation. We assume that

$$G = \mathbb{M}G_0 + z_0,$$

with an orthogonal unit matrix $\mathbb{M}$ and the translation vector z_0.

Consider two integral equations of the first kind

$$\mathbb{H}[g_0](x) = \Phi(x, 0), \quad x \in \partial G_0 \tag{3.1}$$

and

$$\mathbb{H}[g](x) = \Phi(x, z_0), \quad x \in \partial G. \tag{3.2}$$

It has been proven [26] that

LEMMA 3.1. *Assume that $g_0(d)$ is the minimum norm solution of (3.1) with discrepancy $\epsilon > 0$. Then $g(d)$ defined by*

$$g(d) = g_0(\mathbb{M}^{-1}d)e^{-i\kappa d\cdot z_0} \tag{3.3}$$

is the minimum norm solution of (3.2) with discrepancy $\epsilon > 0$.

This result means that we can determine the density function $g(d)$ using the minimum norm solution in the fixed domain G_0 from (3.3) such that

$$\|\mathbb{H}[g](\cdot) - \Phi(\cdot, z_0)\|^2_{L^2(\partial G)} \le \epsilon^2. \tag{3.4}$$

Next, we need to generalize this result to the cases where Φ is replaced by its partial derivative.

For vector-valued function $(\varphi_1, \varphi_2)^T \in L^2(\mathbb{S}) \times L^2(\mathbb{S}) := L^2(\mathbb{S} \times \mathbb{S})$, define

$$\mathbb{H}[(\varphi_1, \varphi_2)^T](x) := (\mathbb{H}[\varphi_1](x), \mathbb{H}[\varphi_2](x))^T.$$

For functions $(f_1, f_2)^T \in L^2(\Gamma) \times L^2(\Gamma) := L^2(\Gamma \times \Gamma)$, we define the norm

$$\|(f_1, f_2)^T\|^2_{L^2(\Gamma\times\Gamma)} := \|f_1\|^2_{L^2(\Gamma)} + \|f_2\|^2_{L^2(\Gamma)},$$

where Γ may be $\mathbb{S}, \partial G_0$ or ∂G.

THEOREM 3.2. *Assume that $f_0^j(d)$ with $j = 1, 2$ are minimum norm solution of*

$$\mathbb{H}[f_0^j](x) = \Phi_{x_j}(x, 0), \quad x \in \partial G_0 \tag{3.5}$$

with discrepancy $\epsilon > 0$. Then the density function $(f^1, f^2)^T$ given by

$$\begin{pmatrix} f^1(d) \\ f^2(d) \end{pmatrix} := \mathbb{M} \begin{pmatrix} f_0^1(\mathbb{M}^{-1}d) \\ f_0^2(\mathbb{M}^{-1}d) \end{pmatrix} e^{-i\kappa d\cdot z_0} \tag{3.6}$$

satisfies that

$$\|\mathbb{H}[(f^1, f^2)^T](\tilde{x}) - (\Phi_{\tilde{x}_1}, \Phi_{\tilde{x}_2})^T(\tilde{x}, z_0)\|^2_{L^2(\partial G)} \le 2\epsilon^2. \tag{3.7}$$

Proof. Using the transform relation, we have $\tilde{x} = \mathbb{M}x + z_0$. Since $|\tilde{x} - z_0| = |\mathbb{M}x| = |x|$, it is easy to show that

$$\begin{pmatrix} \Phi_{\tilde{x}_1}(\tilde{x}, z_0) \\ \Phi_{\tilde{x}_2}(\tilde{x}, z_0) \end{pmatrix} = \mathbb{M} \begin{pmatrix} \Phi_{x_1}(x, 0) \\ \Phi_{x_2}(x, 0) \end{pmatrix}. \tag{3.8}$$

Using (3.6), (3.8) and the property of the orthogonal transform, we get the following estimate

$$\begin{aligned} \|\mathbb{H}[f^1](\cdot) - \Phi_{\tilde{x}_1}(\cdot, z_0)\|^2_{L^2(\partial G)} &= \int_{\partial G} \left| \int_{\mathbb{S}} e^{i\kappa\tilde{x}\cdot d} g^1(d) ds(d) - \Phi_{\tilde{x}_1}(\tilde{x}, z_0) \right|^2 ds(\tilde{x}) \\ = \int_{\partial G_0} \left| \int_{\mathbb{S}} e^{i\kappa z_0\cdot d} e^{i\kappa x\cdot \mathbb{M}^{-1}d} f^1(d) ds(d) - (m_{11}\Phi_{x_1}(x, 0) + m_{12}\Phi_{x_2}(x, 0)) \right|^2 ds(x). \end{aligned}$$

Letting $\mathbb{M}^{-1}d = \tilde{d}$ and using the definition (3.6), we are led to

$$\begin{aligned}
&\|\mathbb{H}[f^1](\cdot) - \Phi_{\tilde{x}_1}(\cdot, z_0)\|^2_{L^2(\partial G)} \\
&= \int_{\partial G_0} \left| \int_{\mathbb{S}} e^{i\kappa z_0 \cdot \mathbb{M}\tilde{d}} e^{i\kappa x\cdot\tilde{d}} f^1(\mathbb{M}\tilde{d}) ds(\tilde{d}) - \sum_{j=1}^{2} m_{1j} \Phi_{x_j}(x,0) \right|^2 ds(x) \\
&= \sum_{j=1}^{2} m_{1j}^2 \int_{\partial G_0} \left| \int_{\mathbb{S}} e^{i\kappa x\cdot\tilde{d}} f_0^j(\tilde{d}) ds(\tilde{d}) - \Phi_{x_j}(x,0) \right|^2 ds(x) + \\
&\quad 2m_{11}m_{12} \int_{\partial G_0} \prod_{j=1}^{2} \left[\int_{\mathbb{S}} e^{i\kappa x\cdot\tilde{d}} f_0^j(\tilde{d}) ds(\tilde{d}) - \Phi_{x_j}(x,0) \right] ds(x) \\
&\le \epsilon^2 + 2m_{11}m_{12} \int_{\partial G_0} \prod_{j=1}^{2} \left[\int_{\mathbb{S}} e^{i\kappa x\cdot\tilde{d}} f_0^j(\tilde{d}) ds(\tilde{d}) - \Phi_{x_j}(x,0) \right] ds(x)
\end{aligned}$$

using $m_{11}^2 + m_{12}^2 = 1$ and the definition of f_0^j. In a similarly way, we get that

$$\begin{aligned}
&\|\mathbb{H}[f^2](\cdot) - \Phi_{\tilde{x}_2}(\cdot, z_0)\|^2_{L^2(\partial G)} \\
&\le \epsilon^2 + 2m_{21}m_{22} \int_{\partial G_0} \prod_{j=1}^{2} \left[\int_{\mathbb{S}} e^{i\kappa x\cdot\tilde{d}} f_0^j(\tilde{d}) ds(\tilde{d}) - \Phi_{x_j}(x,0) \right] ds(x).
\end{aligned}$$

Noticing that $m_{11}m_{12} + m_{21}m_{22} = 0$, we finally get (3.19) by summing up these two estimates. The proof is complete. □

Compared with Lemma 3.1, this result is its generalization in some weak sense, that is, we can not assert $(f^1(d), f^2(d))$ is the minimum norm solution of

$$\mathbb{H}[(\varphi^1, \varphi^2)^T](\tilde{x}) = (\Phi_{\tilde{x}_1}, \Phi_{\tilde{x}_2})^T(\tilde{x}, z_0), \quad \tilde{x} \in \partial G \tag{3.9}$$

with discrepancy $\sqrt{2}\epsilon$. Fortunately, such a weak generalization is enough for our purpose. On the other hand, the discrepancy level $\sqrt{2}\epsilon$ is optimal for the density function given by (3.6).

A small change of the assumptions on $f_0^j(d)$ can guarantee that $(f^1(d), f^2(d))$ is the minimum norm solution of (3.9). This is the following counterpart of Lemma 3.1.

THEOREM 3.3. *Assume that the vector-valued function $(f_0^1(d), f_0^2(d)) \in L^2(\mathbb{S}\times\mathbb{S})$ is the minimum norm solution of*

$$\mathbb{H}[(\varphi^1, \varphi^2)^T](x) = (\Phi_{x_1}, \Phi_{x_2})^T(x, 0), \quad x \in \partial G_0 \tag{3.10}$$

with discrepancy $\epsilon > 0$. Then the density function $(f^1, f^2)^T$ given by (3.6) is the minimum norm solution of equation (3.9) with discrepancy $\epsilon > 0$.

Proof. The computation in the proof of the above theorem yields that

$$\begin{cases}
\|\mathbb{H}[f^1](\cdot) - \Phi_{\tilde{x}_1}(\cdot, z_0)\|^2_{L^2(\partial G)} = \sum_{j=1}^{2} m_{1j}^2 \|\mathbb{H}[f_0^j](\cdot) - \Phi_{x_j}(x,0)\|^2_{L^2(\partial G_0)} + \\
\qquad 2m_{11}m_{12} \int_{\partial G_0} \prod_{j=1}^{2} \left[\int_{\mathbb{S}} e^{i\kappa x\cdot\tilde{d}} f_0^j(\tilde{d}) ds(\tilde{d}) - \Phi_{x_j}(x,0) \right] ds(x), \\
\|\mathbb{H}[f^2](\cdot) - \Phi_{\tilde{x}_2}(\cdot, z_0)\|^2_{L^2(\partial G)} = \sum_{j=1}^{2} m_{2j}^2 \|\mathbb{H}[f_0^j](\cdot) - \Phi_{x_j}(x,0)\|^2_{L^2(\partial G_0)} + \\
\qquad 2m_{21}m_{22} \int_{\partial G_0} \prod_{j=1}^{2} \left[\int_{\mathbb{S}} e^{i\kappa x\cdot\tilde{d}} f_0^j(\tilde{d}) ds(\tilde{d}) - \Phi_{x_j}(x,0) \right] ds(x).
\end{cases}$$

Summing up these two identities and noticing $m_{11}m_{12}+m_{21}m_{22}=0$, we get that

$$\begin{aligned}&\|\mathbb{H}[(f^1,f^2)^T](\cdot)-(\Phi_{\tilde{x}_1},\Phi_{\tilde{x}_2})^T(\cdot,z_0)\|^2_{L^2(\partial G\times\partial G)}\\&=\sum_{j=1}^{2}m_{1j}^2\|\mathbb{H}[f_0^j](\cdot)-\Phi_{x_j}(\cdot,0)\|^2_{L^2(\partial G_0)}+\sum_{j=1}^{2}m_{2j}^2\|\mathbb{H}[f_0^j](\cdot)-\Phi_{x_j}(\cdot,0)\|^2_{L^2(\partial G_0)}.\end{aligned}$$

Using the property $m_{11}=m_{22}, m_{12}=-m_{21}$ and $m_{11}^2+m_{12}^2=1$, the above equality becomes by exchanging the order of summation

$$\begin{aligned}&\|\mathbb{H}[(f^1,f^2)^T](\cdot)-(\Phi_{\tilde{x}_1},\Phi_{\tilde{x}_2})^T(\cdot,z_0)\|^2_{L^2(\partial G\times\partial G)}=\sum_{j=1}^{2}\|\mathbb{H}[f_0^j](\cdot)-\Phi_{x_j}(\cdot,0)\|^2_{L^2(\partial G_0)}\\&=\|\mathbb{H}[(f_0^1,f_0^2)^T](\cdot)-(\Phi_{x_1},\Phi_{x_2})^T(\cdot,0)\|^2_{L^2(\partial G_0\times\partial G_0)}\le\epsilon^2\end{aligned}$$

from the definition of (f_0^1,f_0^2). That is, (f^1,f^2) is an approximate solution of (3.9) with discrepancy ϵ.

Next, we prove that $(f_1,f_2)^T$ is also the minimum norm solution of (3.9) with discrepancy ϵ. If this argument is not true, then there exists another function $(\tilde{f}_1,\tilde{f}_2)\in L^2(\mathbb{S}\times\mathbb{S})$, which is the minimum norm solution of (3.9) with discrepancy ϵ. That is, $(\tilde{f}_1,\tilde{f}_2)$ meets

$$\|\mathbb{H}[(\tilde{f}^1,\tilde{f}^2)](\cdot)-(\Phi_{\tilde{x}_1},\Phi_{\tilde{x}_2})^T(\cdot,z_0)\|^2_{L^2(\partial G\times\partial G)}\le\epsilon^2 \tag{3.11}$$

and

$$\|(\tilde{f}^1,\tilde{f}^2)\|^2_{L^2(\mathbb{S}\times\mathbb{S})}<\|(f^1,f^2)\|^2_{L^2(\mathbb{S}\times\mathbb{S})}. \tag{3.12}$$

Now we construct $(\tilde{f}_0^1,\tilde{f}_0^2)\in L^2(\mathbb{S}\times\mathbb{S})$ by

$$\begin{pmatrix}\tilde{f}_0^1(d)\\ \tilde{f}_0^2(d)\end{pmatrix}:=\mathbb{M}^{-1}\begin{pmatrix}\tilde{f}^1(\mathbb{M}d)\\ \tilde{f}^2(\mathbb{M}d)\end{pmatrix}e^{i\kappa\mathbb{M}d\cdot z_0}. \tag{3.13}$$

By direct computation using the transform relation and (3.11), we can derive that

$$\|\mathbb{H}[(\tilde{f}_0^1,\tilde{f}_0^2)](\cdot)-(\Phi_{x_1},\Phi_{x_2})^T(\cdot,z_0)\|^2_{L^2(\partial G_0\times\partial G_0)}\le\epsilon^2. \tag{3.14}$$

On the other hand, using the definitions (3.6) and (3.13), we can prove that

$$\|(\tilde{f}_0^1,\tilde{f}_0^2)^T\|_{L^2(\mathbb{S}\times\mathbb{S})}=\|(\tilde{f}^1,\tilde{f}^2)^T\|_{L^2(\mathbb{S}\times\mathbb{S})},\quad \|(f_0^1,f_0^2)^T\|_{L^2(\mathbb{S}\times\mathbb{S})}=\|(f^1,f^2)^T\|_{L^2(\mathbb{S}\times\mathbb{S})}.$$

Therefore (3.12) yields

$$\|(\tilde{f}_0^1,\tilde{f}_0^2)^T\|^2_{L^2(\mathbb{S}\times\mathbb{S})}<\|(f_0^1,f_0^2)^T\|^2_{L^2(\mathbb{S}\times\mathbb{S})}. \tag{3.15}$$

Combining (3.14) and (3.15), we conclude that $(f_0^1,f_0^2)^T$ is not the minimum norm solution of (3.10) with discrepancy ϵ, which is a contradiction. □

Comparing Theorem 3.2 and Theorem 3.3, both of them can be used to construct the approximation of $\Phi_{x_j}(\tilde{x},z_0)$ in ∂G from the minimum norm solution in the reference domain ∂G_0. However, in order to guarantee that (f^1,f^2) is the minimum norm solution, we need to solve the density (f_0^1,f_0^2) as the minimum norm solution from the coupled equation (3.10), which will leads to large amount of computation since $\mathbb{H}$

is defined in $L^2(\mathbb{S}) \times L^2(\mathbb{S})$ in this case. Therefore, from the numerical point of view, Theorem 3.1 is more suitable for the approximation.

For the second derivative of the fundamental solution, we have similar results.

THEOREM 3.4. *Define $\mathbb{Q} = \mathbb{M}^2$. Assume that $h_0^j(d)$ with $j = 1, 2$ are minimum norm solutions of*

$$\mathbb{H}[h_0^j](x) = \Phi_{x_j x_2}(x, 0), \quad x \in \partial G_0 \tag{3.16}$$

with discrepancy $\epsilon > 0$. Then the density function $(h^1, h^2)^T$ given by

$$\begin{pmatrix} h^1(d) \\ h^2(d) \end{pmatrix} := \mathbb{Q} \begin{pmatrix} h_0^1(\mathbb{Q}^{-1}d) \\ h_0^2(\mathbb{Q}^{-1}d) \end{pmatrix} e^{-i\kappa d \cdot z_0} \tag{3.17}$$

satisfies that

$$\|\mathbb{H}[(h^1, h^2)^T](\cdot) - (\Phi_{\tilde{x}_1 \tilde{x}_2}, \Phi_{\tilde{x}_2 \tilde{x}_2})^T(\cdot, z_0)\|^2_{L^2(\partial G \times \partial G)} \leq 2\epsilon^2. \tag{3.18}$$

Proof. It follows from (3.8) and the fact that $\Phi_{x_1 x_1}(x, 0) + \Phi_{x_2 x_2}(x, 0) \equiv 0$ that

$$\begin{aligned} \begin{pmatrix} \Phi_{\tilde{x}_1 \tilde{x}_2}(\tilde{x}, z_0) \\ \Phi_{\tilde{x}_2 \tilde{x}_2}(\tilde{x}, z_0) \end{pmatrix} &= \mathbb{M} \frac{\partial}{\partial \tilde{x}_2} \begin{pmatrix} \Phi_{x_1}(x, 0) \\ \Phi_{x_2}(x, 0) \end{pmatrix} = \mathbb{M} \begin{pmatrix} \frac{\partial x_2}{\partial \tilde{x}_2} & -\frac{\partial x_1}{\partial \tilde{x}_2} \\ \frac{\partial x_1}{\partial \tilde{x}_2} & -\frac{\partial x_2}{\partial \tilde{x}_2} \end{pmatrix} \begin{pmatrix} \Phi_{x_1 x_2}(x, 0) \\ \Phi_{x_2 x_2}(x, 0) \end{pmatrix} \\ &= \mathbb{M}^2 \begin{pmatrix} \Phi_{x_1 x_2}(x, 0) \\ \Phi_{x_2 x_2}(x, 0) \end{pmatrix}. \end{aligned} \tag{3.19}$$

Define $\mathbb{Q} = \mathbb{M}^2$, then the proof is the same as Theorem 3.2. □

The counterpart of Theorem 3.3 is also true for (h^1, h^2).

From the above results, we get the following

COROLLARY 3.5. *Assume that g_0, f_0^j, h_0^j are the minimum norm solution of equations (3.1), (3.5) and (3.16) with discrepancy ϵ in the fixed reference domain ∂G_0, respectively. Then the density functions g, f^j, h^j constructed by (3.3), (3.6) and (3.17) respectively meet*

$$\|\mathbb{H}[g](\cdot) - \Phi(\cdot, z_0)\|, \ \|\mathbb{H}[f^j](\cdot) - \Phi_{x_j}(\cdot, z_0)\|, \ \|\mathbb{H}[h^j](\cdot) - \Phi_{x_j x_2}(\cdot, z_0)\| \leq \sqrt{2}\epsilon \tag{3.20}$$

for $j = 1, 2$, where the norm is in $L^2(\partial G)$ and $G = \mathbb{M}G_0 + z_0$.

Using this result, we can approximate the singular source by Herglotz wave functions in all approximate domains $\partial D_a^p := \mathbb{M}(a)D_0 + z_p$ with a few amount of computations, where $\mathbb{M}(a)$ represents the approaching direction and z_p the approaching step along this direction. When we choose different rotation matrix $\mathbb{M}(a)$ and approaching points z_p from a fixed reference domain D_0, $z_p \notin D_a^p$ can approach to any points $a \in \partial D$. Once we compute the minimum norm solution φ_0 in the fixed reference domain ∂D_0, the density functions for approaching singular source in ∂D_a^p can be computed from φ_0 by a simple function transformation. Using this way, the numerical realizations of probe method can be implemented efficiently. A geometric configuration of the reference domain D_0 with some cone shape boundary and its transform is shown in Figure 3.1.

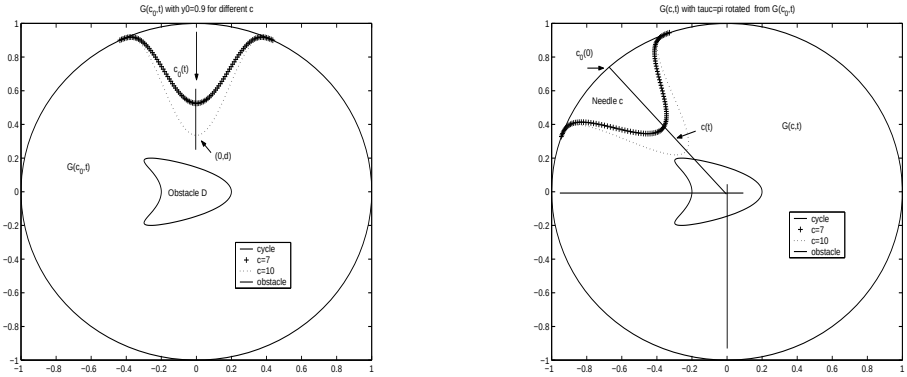

FIG. 3.1. *A possible configuration of reference domain D_0 (left) and its rigid transform by rotation and translation (right).*

4. Error estimates on the singular source approximation. When we decompose the singular sources such as $\Phi(x, z_p), \partial_{x_j}\Phi(x, z_p), \partial_{x_j x_2}\Phi(x, z_p)$ with $j = 1, 2$ approximately into the superposition of incident plan wave in ∂D_a^p, we need to solve an integral equation of the first kind

$$\mathbb{H}[\varphi](x) = F(x, 0), \quad x \in \partial G_0 \tag{4.1}$$

in the boundary of reference domain G_0, where we assume that $0 \notin \overline{G}_0$ and $F(x, 0)$ represents $\Phi(x, 0), \partial_{x_j}\Phi(x, 0)$ or $\partial_{x_j x_2}\Phi(x, 0)$. The theoretical results in section 3 assert that the approximation accuracy in every approximate domain ∂D_a^p is essentially determined by the solution (4.1), since the function transform for the density with an analytic expression does not generate extra error.

Compared with general integral equation of the first kind, the difficulty of solving (4.1) by regularization is that the right-hand side of (4.1) is almost a singular function for $x \in \partial G_0$ near 0. Therefore we need to estimate the influence of such a singularity on the numerical solution. More precisely, the relation between the singularity strength of $F(x, 0)$, the choice of regularizing parameter α and the discrete number n for dividing ∂G_0 and $\mathbb{S}$ in solving (4.1) should be analyzed.

The minimum norm solution $\varphi_\epsilon(d)$ of (4.1) with discrepancy $\epsilon > 0$ is obtained by solving the equation

$$\alpha\varphi^\alpha(d) + \mathbb{H}^*\mathbb{H}[\varphi^\alpha](d) = \mathbb{H}^*[F](d), \quad d \in \mathbb{S}, \tag{4.2}$$

where the regularizing parameter $\alpha = \alpha(\epsilon)$ is determined by the Morozov discrepancy principle

$$\|\mathbb{H}[\varphi^\alpha](\cdot) - F(\cdot, 0)\|_{L^2(\partial G_0)} = \epsilon. \tag{4.3}$$

That is, $\varphi_\epsilon = \varphi^{\alpha(\epsilon)}$ with $\varphi^{\alpha(\epsilon)}$ determined from (4.2) and (4.3). We need to estimate $\|\mathbb{H}[\varphi_{\epsilon,N}] - F\|_{L^2(\partial G_0)}$, where $\varphi_{\epsilon,N}$ is the finite dimensional approximation to $\varphi_\epsilon \in L^2(\mathbb{S})$.

Introduce the finite dimensional subspace $X_n \subset L^2(\mathbb{S}), Y_n \subset L^2(\partial G_0)$. Denote by φ_n, F_n the projection of $\varphi \in L^2(\mathbb{S}), F \in L^2(\partial G_0)$ into X_n, Y_n, respectively. Then for any fixed $\alpha > 0$, it is well-known for the regularizing equation (4.2) that

$$\|\varphi_n^\alpha - \varphi^\alpha\|_{L^2(\mathbb{S})} \le \frac{1}{2\sqrt{\alpha}}\|F_n - F\|_{L^2(\partial G_0)}. \tag{4.4}$$

Therefore the approximation to the density function with minimum norm meets

$$\|\varphi_{\epsilon,n} - \varphi_\epsilon\|_{L^2(\mathbb{S})} \leq \frac{1}{2\sqrt{\alpha(\epsilon)}}\|F_n - F\|_{L^2(\partial G_0)}. \tag{4.5}$$

Finally, we have the estimate

$$\begin{aligned}\|\mathbb{H}[\varphi_{\epsilon,N}] - F\|_{L^2(\partial G_0)} &\leq \|\mathbb{H}[\varphi_{\epsilon,n} - \varphi_\epsilon]\|_{L^2(\partial G_0)} + \|\mathbb{H}[\varphi_\epsilon] - F\|_{L^2(\partial G_0)} \\ &\leq \|\mathbb{H}\|_{L^2}\frac{1}{2\sqrt{\alpha(\epsilon)}}\|F_n - F\|_{L^2(\partial G_0)} + \epsilon. \end{aligned}\tag{4.6}$$

This estimate reveals that the approximation accuracy of the singular source function by Herglotz wave function in a finite dimensional space depends on the balance of $\frac{1}{2\sqrt{\alpha(\epsilon)}}\|F_n - F\|_{L^2(\partial G_0)}$ and ϵ. We state the above analysis as the following

THEOREM 4.1. *Assume that $\|F(\cdot,0)\|_{L^2(\partial G_0)} > \epsilon$ and $\alpha(\epsilon)$ is the regularizing parameter related to minimum norm solution of (4.1) with discrepancy ϵ. If the dimension $n := n(\epsilon)$ is chosen to meet*

$$\|F_n - F\|_{L^2(\partial G_0)} = O(\epsilon\sqrt{\alpha(\epsilon)}), \tag{4.7}$$

then the error for the singular source approximation using the Herglotz wave function with the density function in finite dimensional space X_n satisfies the estimate

$$\|\mathbb{H}[\varphi_{\epsilon,n}] - F\|_{L^2(\partial G_0)} = O(\epsilon) \text{ as } \epsilon \to 0.$$

This estimate gives us a theoretical criterion for taking the dimension of the approximate function subspace. From the standard estimate [21]

$$0 < \alpha(\epsilon) \leq \frac{\|\mathbb{H}^*\|\epsilon}{\|F(\cdot,0)\|_{L^2(\partial G_0)} - \epsilon}, \tag{4.8}$$

we know that $\alpha(\epsilon) \to 0$ at least linearly with respect to ϵ. Therefore we need to chose the dimension $n = n(\epsilon)$ of projection subspace Y_n to satisfy at least $\|F_n - F\|_{L^2(\partial G_0)} = O(\epsilon^{3/2})$ to guarantee the approximation. Noticing that the smoothness of $F(x,0)$ is not uniform in ∂G_0, see Figure 4.1, it is preferable to take non uniform mesh to meet this requirement. If uniform mesh is taken, then n must be quite large for small ϵ.

To determine the exact $\alpha(\epsilon)$, we need to solve a nonlinear equation constituted by (4.2) and (4.3), which is time-consuming. However, our numerical experiences show that a rough choice

$$\alpha(\epsilon) := \frac{\beta\|\mathbb{H}^*\|\epsilon}{\|F(\cdot,0)\|_{L^2(\partial G_0)} - \epsilon}$$

for fixed $\beta \in (0,1)$ is applicable for our singular source approximation. In fact, in numerical implementations given in the next section, we take $\beta = 10^{-l}$ with $l = 1,2,3$ and chose one of them such that the approximation to $F(x,0)$ with minimum discrepancy.

Since the probe method uses the singularity of fundamental solution in the pointwise sense to detect the obstacle boundary, we need to estimate the approximation error $\mathbb{H}[\varphi_{\epsilon,n}](x) - F(x,0)$ in the finite dimensional space in the $L^\infty-$sense. Of course,

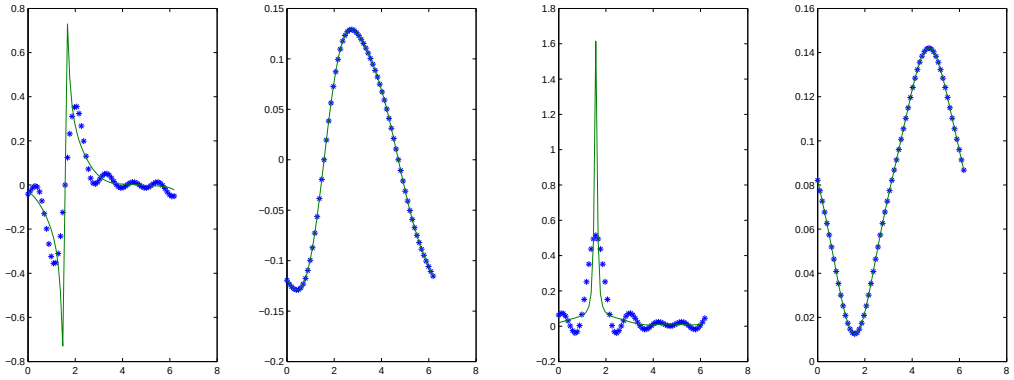

FIG. 4.1. *The singular behaviors of $\Phi_{x_1}(x, z_0)$ (left) and $\Phi_{x_2}(x, z_0)$ (right) in a circle $|x| = R_0$ with $z_0 = (0, R_0 + \delta_0)$ for small δ_0, together with their approximations shown in star line using uniform mesh. The imaginary parts of $\Phi_{x_i}(x, z_0)$ are quite smooth and therefore can be approximated well.*

this error depends on the error $\|\mathbb{H}[\varphi_\epsilon](\cdot) - F(\cdot, 0)\|_{L^\infty}$. We give this dependence by the following

THEOREM 4.2. *Assume that $\|F(\cdot, 0)\|_{L^2(\partial G_0)} > \epsilon$ and $\alpha(\epsilon)$ is the regularizing parameter related to minimum norm solution of (4.1) with discrepancy ϵ. Then the $L^\infty-$error for the singular source approximation using the density function in finite dimensional space X_n satisfies*

$$\left|\|\mathbb{H}[\varphi_{\epsilon,n}] - F\|_{L^\infty(\partial G_0)} - \|\mathbb{H}[\varphi_\epsilon] - F\|_{L^\infty(\partial G_0)}\right| < \frac{C_0}{\sqrt{\alpha(\epsilon)^3}}\|F_n - F\|_{L^\infty(\partial G_0)}, \quad (4.9)$$

where the constant $C_0 = C_0(\mathbb{H}, \partial G_0)$.

Proof. Using the triangle inequality, it follows that

$$\begin{aligned}\|\mathbb{H}[\varphi_{\epsilon,n}] - F\|_{L^\infty(\partial G_0)} &\le \|\mathbb{H}[\varphi_{\epsilon,n} - \varphi_\epsilon]\|_{L^\infty(\partial G_0)} + \|\mathbb{H}[\varphi_\epsilon] - F\|_{L^\infty(\partial G_0)} \\ &\le \|\mathbb{H}\|_\infty\|\varphi_{\epsilon,n} - \varphi_\epsilon\|_{L^\infty(\mathbb{S})} + \|\mathbb{H}[\varphi_\epsilon] - F\|_{L^\infty(\partial G_0)}. \quad (4.10)\end{aligned}$$

Now let us estimate $\|\varphi_{\epsilon,n} - \varphi_\epsilon\|_{L^\infty(\mathbb{S})}$. Define $\psi_n(d) := \varphi_{\epsilon,n}(d) - \varphi_\epsilon(d), f_n(x) := F_n(x, 0) - F(x, 0)$ for the simplicity of notation. It is easy to see that

$$\alpha\psi_n(d) + \mathbb{H}^*\mathbb{H}[\psi_n](d) = \mathbb{H}^*[f_n](d), \quad d \in \mathbb{S}, \quad (4.11)$$

which means that

$$\|\psi_n\|_{L^\infty(\mathbb{S})} \le \|(\alpha\mathbb{I} + \mathbb{H}^*\mathbb{H})^{-1}\mathbb{H}^*\|_\infty\|f_n\|_{L^\infty(\partial G_0)}. \quad (4.12)$$

We claim that

$$\|(\alpha\mathbb{I} + \mathbb{H}^*\mathbb{H})^{-1}\mathbb{H}^*\|_\infty \le \frac{\|\mathbb{H}^*\|_\infty(\sqrt{|\partial G_0||\mathbb{S}|} + 2)}{\sqrt{\alpha^3}}. \quad (4.13)$$

In fact, assume that $(\alpha\mathbb{I} + \mathbb{H}^*\mathbb{H})^{-1}\mathbb{H}^*w = \psi$ in $\mathbb{S}$, then it follows from the standard estimate of Tikhonov regularization in L^2 setting that

$$\|\psi\|_{L^2(\mathbb{S})} \le \|(\alpha\mathbb{I} + \mathbb{H}^*\mathbb{H})^{-1}\mathbb{H}^*\|_{L^2}\|w\|_{L^2(\partial G_0)} \le \frac{\sqrt{|\partial G_0|}}{2\sqrt{\alpha}}\|w\|_\infty.$$

On the other hand, we get from $(\alpha\mathbb{I}+\mathbb{H}^*\mathbb{H})\psi=\mathbb{H}^*w$ that

$$\|\psi\|_\infty \le \frac{1}{\alpha}\left[\|\mathbb{H}^*w\|_\infty+\|\mathbb{H}^*\mathbb{H}\psi\|_\infty\right] \le \frac{\|\mathbb{H}^*\|_\infty}{\alpha}\left[\|w\|_\infty+\|\mathbb{H}\psi\|_\infty\right].$$

From the definition of $\mathbb{H}$, it is easy to see that

$$|\mathbb{H}[\psi](x)| \le \int_{\mathbb{S}} |e^{i\kappa d\cdot x}\psi(d)|ds(d) \le \sqrt{|\mathbb{S}|}\|\psi\|_{L^2(\mathbb{S})}.$$

The above three estimates lead to (4.13).

Inserting (4.13) and (4.12) into (4.10) says

$$\|\mathbb{H}[\varphi_{\epsilon,n}]-F\|_{L^\infty(\partial G_0)} \le \|\mathbb{H}\|_\infty \frac{C_0}{\sqrt{\alpha(\epsilon)^3}} + \|\mathbb{H}[\varphi_\epsilon]-F\|_{L^\infty(\partial G_0)}.$$

Exchanging the position of $\varphi_{\epsilon,n}$ and φ_ϵ in this relation and combining these two relations together, the proof is complete. □

REMARK 4.3. *The fact that the discrete error $\|\mathbb{H}[\varphi_{\epsilon,n}]-F\|_{L^\infty(\partial G_0)}$ depends on its continuous version $\|\mathbb{H}[\varphi_\epsilon]-F\|_{L^\infty(\partial G_0)}$ is obvious. The importance of this theorem is the relation of these two terms. Compared with the L^2-norm estimate given in the previous theorem, this theorem states that we need to take more large $n:=n(\epsilon)$ to get the same error as that of the measurement by L^2-norm. It is generally impossible to estimate $\|\mathbb{H}[\varphi_{\epsilon,n}]-F\|_{L^\infty(\partial G_0)}$ by ϵ explicitly, since we only have the estimate $\|\mathbb{H}[\varphi_\epsilon]-F\|_{L^2(\partial G_0)}<\epsilon$.*

5. Numerical implementations. We give the numerics to test the algorithm. In all the numerical tests, we take wave number $\kappa=1.2$ and use far-field pattern data along 64 directions. The detection of the obstacle boundary is also along 64 directions uniformly distributed in $[0,2\pi]$.

We use (2.20) to detect the boundary. Here we focus on the effect of surface impedance and the obstacle curvature.

Example 1. Take D being a cycle

$$\partial D := \{x=1.5(\cos t,\sin t), t\in[0,2\pi]\}.$$

Step 1. Firstly we choose the surface impedance as a real constant. For this special case with a constant curvature, we consider the case that ∂D has a mixed boundary $\partial D_D=\{x\in\partial D: t\in[0,\pi)\}$, $\partial D_I=\{x\in\partial D: t\in(\pi,2\pi]\}$.

We take singularity $\delta_1=0.01$ and the approaching steps $\delta_0=0.02$ for $l=16,\cdots,1$. That is, along each direction, the approaching radius is $1.5+l\times\delta_0+\delta_1$.

The results for $\sigma(x)=30, \sigma(x)=3$ using the same blowing-up criterion in all directions are shown in Figure 5.1. For large σ (left) which implies the impedance boundary is almost a Dirichlet boundary, the whole obstacle is detected well, see the first picture in Figure 5.1. However, for small $\sigma(x)$ (right), the blowing-up behavior for the impedance boundary is weak. Using the same blowing up criterion in all directions, the impedance part can not be detected, that is, all detection points of the impedance boundary are just the initial guess, see the second picture in Figure 5.1. This numerical test reveals that the same blowing-up criterion can not be used for the mixed boundary condition, provide that $\sigma^r(x)$ be not so large.

Step 2. To explain the effect of surface impedance in the whole boundary clearly, we assume $\partial D=\partial D_I$ and consider three cases:

$$\sigma(x)=5-5i, \quad \sigma(x)=5-\frac{0.6667}{\kappa}i, \quad \sigma(x)=5-5\sin(6x_1x_2)i$$

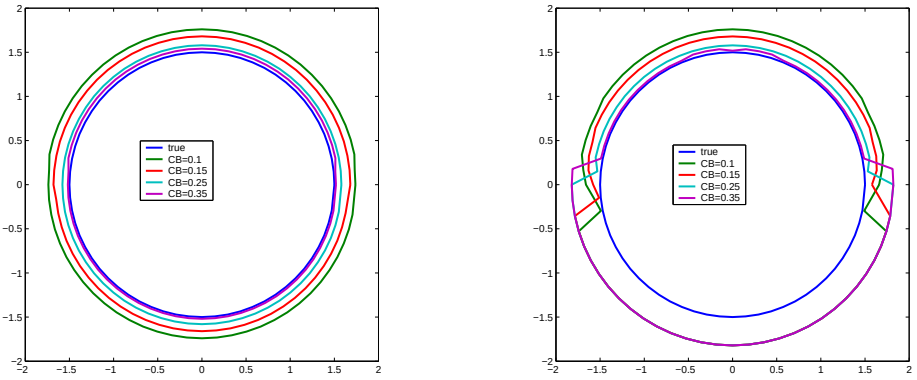

FIG. 5.1. *Reconstruction of ∂D for mixed boundary condition with $\sigma(x) = 30$ (left) and $\sigma(x) = 3$ (right) in ∂D_I, using the uniform blowing-up criteria in all directions.*

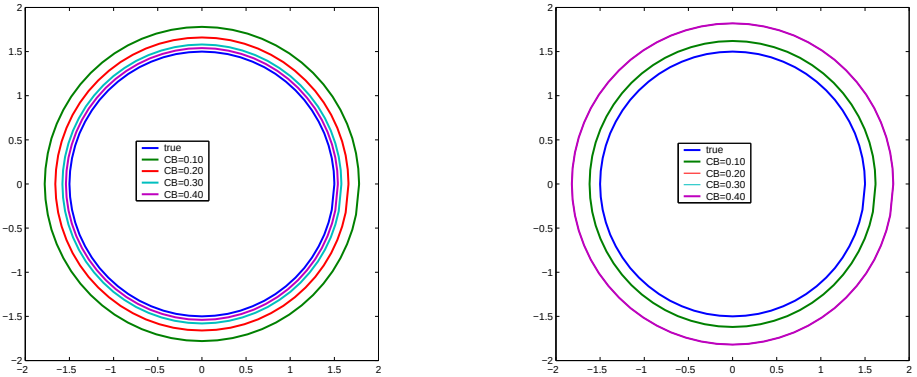

FIG. 5.2. *Reconstruction of ∂D for surface impedance in ∂D with $\sigma(x) = 5 - 5i$ (left) and $\sigma(x) = 5 - \frac{0.6667}{1.2}i$ (right), using the uniform blowing-up criteria in all directions. For large blowing-up values, the boundary can not be seen (right).*

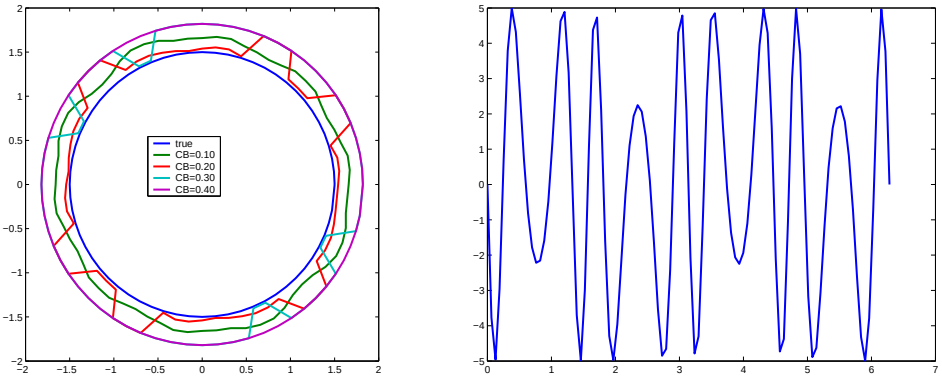

FIG. 5.3. *Reconstruction of ∂D for surface impedance with oscillatory imaginary part(left), and the function of $\operatorname{Im}\sigma(x)$(right). The formula (2.20) can be used to explain this reconstruction. That is, the oscillation of $\sigma^i(x)$ in ∂D_I decreases the visibility of obstacle.*

distributed in the whole boundary. The second case meets $f''(a)+\kappa\sigma^i(a)\equiv 0$ in ∂D_I. Notice, it has been shown in Step 1 that the blowing-up criterion can not be chosen as the same value in all directions for the mixed boundary condition.

We take $\delta_0 = \delta_1 = 0.02$. Using different uniform blowing-up values, the reconstructions are given in Figure 5.2 for the first two configurations. We see that the whole obstacle can be seen for both cases. However, the reconstruction is better in the picture of the left hand side. This is natural and it can be explained using (2.29). Indeed, for the picture in the left side, we have $f''(a)+\kappa\sigma^i(a) = -5\kappa+0.6667$ on ∂D which is negative and quite large while for the picture in the right hand side we have $f''(a)+\kappa\sigma^i(a) = 0$ on ∂D. For both sides, the blowup is mostly uniform, however the one corresponding to the first example is weaker than the one corresponding to the second example. So, using the same blowing-up value, the points for which the indicator function of the first example reaches them are closer to ∂D than the ones corresponding to the indicator function of the second example.

The reconstructions with oscillatory $\sigma^i(x)$ (the third case) are shown in Figure 5.3. It can be seen that the oscillation of $\sigma^i(x)$ on ∂D makes the obstacle less visible. In addition, for large blowing-up values of CB, we cannot recognize at all the very well uniform shape of a circle.

Next we consider a convex obstacle with a varying curvature.

Example 2. Take D being a ellipse $\partial D := \{x = (2\cos t, \sin t), t \in [0, 2\pi]\}$, and assume that ∂D is surface impedance boundary.

We show that this obstacle will be more visible by introducing suitable complex variable surface impedance $\sigma(x) = 5 + \sigma^i(x)i$.

To compare the results, we take the same value $\delta_0 = 0.02, \delta_1 = 0.01$ for the singularity and use the same blowing-up criteria $CB = 0.10, 0.15, 0.20, 0.25$ respectively, for different surface impedance. Define

$$f''(x) := \frac{x_1'(t)x_2''(t) - x_1''(t)x_2'(t)}{(x_1'(t)^2 + x_2'(t))^{3/2}},$$

the curvature of ∂D at point $x = x(t) \in \partial D$.

The reconstructions for the configuration $\sigma^i(x) \equiv 0$ and $f''(x) + \kappa\sigma^i(x) = 0$ are given in Figure 5.4, while the reconstruction for $f''(x) + \kappa\sigma^i(x) = -3$ and $f''(x) + \kappa\sigma^i(x) = -10$ are given in Figure 5.5.

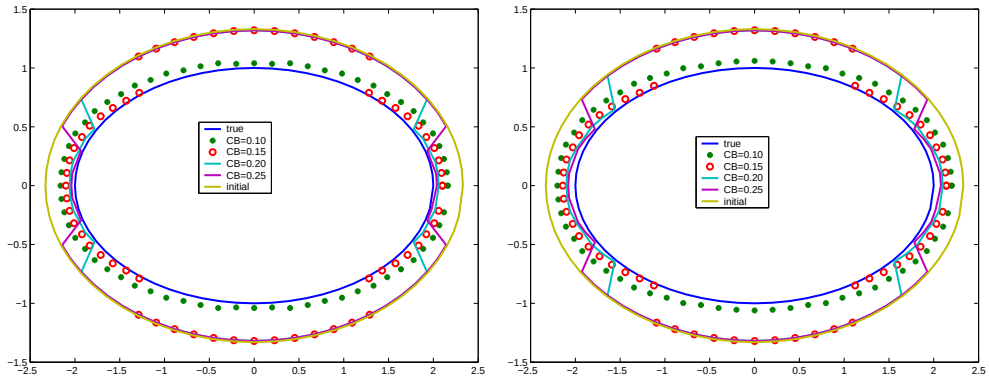

FIG. 5.4. *Reconstructions for $\sigma^i(x) \equiv 0$ (left) and for variable imaginary surface satisfying $f'' + \kappa\sigma^i \equiv 0$ in ∂D (right).*

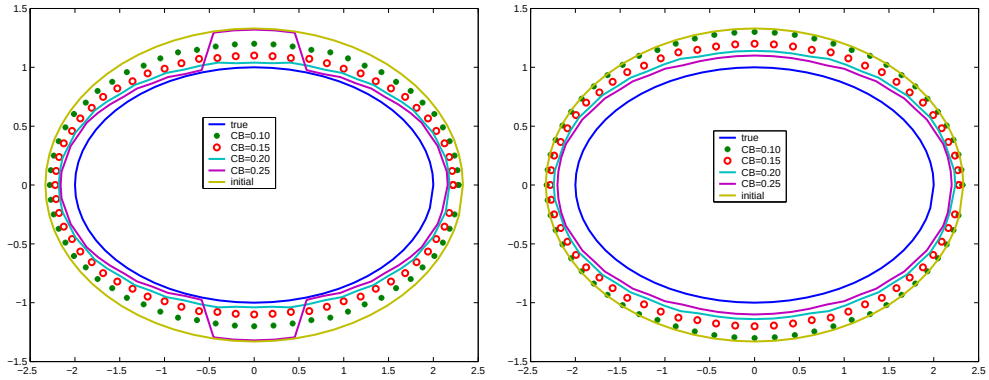

FIG. 5.5. *Reconstructions for variable imaginary surface satisfying* $f''(x) + \kappa\sigma^i(x) \equiv -3$ *(left) and* $f''(x) + \kappa\sigma^i(x) \equiv -10$ *(right) in* ∂D.

Comparing the reconstruction behaviors presented in Figure 5.4 and Figure 5.5, we can see clearly how the introduction of imaginary part of surface impedance makes the obstacle more uniformly visible step by step. That is, in the right-hand side of Figure 5.5, the strong visibility near $t = 0$ and $t = \pi$ due to the large curvature has been relatively weakened, or equivalently, the visibility near $t = \pi/2$ and $t = 3\pi/2$ is relatively enhanced. The whole boundary has an uniform visibility. That is, all points of the boundary are reconstructed in almost the same accuracy. Notice that using the largest blowing-up value $CB = 0.25$ with $\sigma^i(x) \equiv 0$, it can detect the small part with largest curvature (near $t = 0, \pi$) almost exactly, but see nothing in the other part. However, when we introduce $f''(x) + \kappa\sigma^i(x) \equiv -10$, the same blowing-up value can detect the whole boundary uniformly, with a cost of relatively small accuracy in the part with largest curvature. Moreover, it is also the best reconstruction compared with the other small indicator value shown in the second picture of Figure 5.5. This can be explained in the same way as we did in Figure 5.3 using (2.29).

Example 3. Consider a complex obstacle

$$\partial D = \{x : x(t) = (x_1(t), x_2(t)) = (\cos t + 0.65\cos 2t - 0.65, 1.5\sin t), t \in [0, 2\pi]\},$$

which contains concave part and a large oscillation of the curvature. The obstacle as well as its curvature distribution is shown in Figure 5.6.

Step 1. We consider the constant surface impedance using the approaching parameters $\delta_0 = \delta_1 = 0.02$. The reconstruction for $\sigma(x) = 5, \sigma(x) = 5 - 5i$ are shown in Figure 5.7.

Of course, the blowing-up criterion is not uniform in all directions for this configuration, since the impedance is constant and the geometric shape has essential difference in the different part of the boundary. This phenomena is revealed in the reconstruction. For the same blowing-up value, the best reconstructions are obtained near A, B due to the large curvature and therefore the strong scattering. Obviously, if a large blowing-up values ($CB = 0.2, 0.3, 0.4$) are given, then most of the boundary part with small curvature can not be reconstructed due to weak scattering. On the other hand, the introduction of the constant imaginary part improves the uniform property, but not so satisfactory.

As we have explained, the non-uniform blowing up property comes from the different curvature. Now let us consider the curvature effect when the imaginary

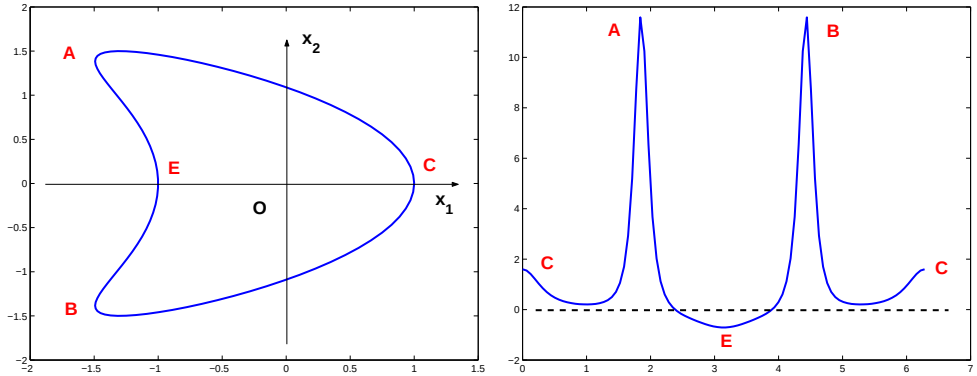

FIG. 5.6. *A kite-shaped obstacle (left) and its curvature distribution with respect to the polar angle (right). The curvature takes maximum value near points A, B, which means a strong scattering in this part.*

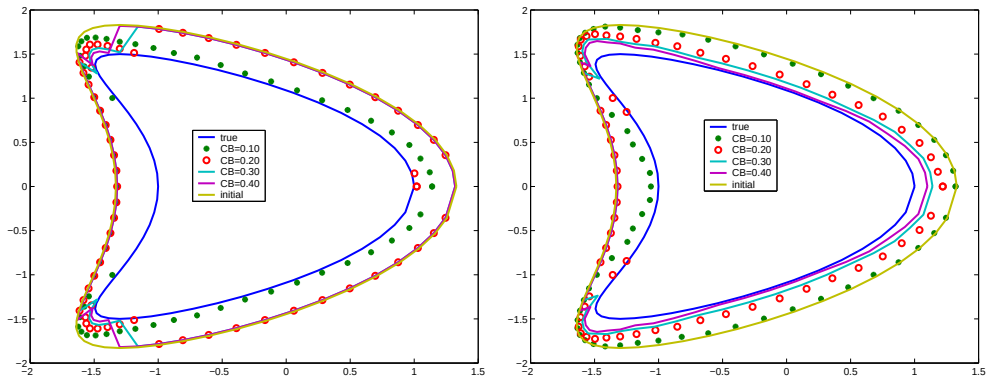

FIG. 5.7. *Reconstruction for the constant surface impedance $\sigma(x) \equiv 5$ (left) and $\sigma(x) \equiv 5 - 5i$ (right). For real surface impedance, the part of the boundary with the maximum curvature is relatively easy to be detected for the same blowing-up value.*

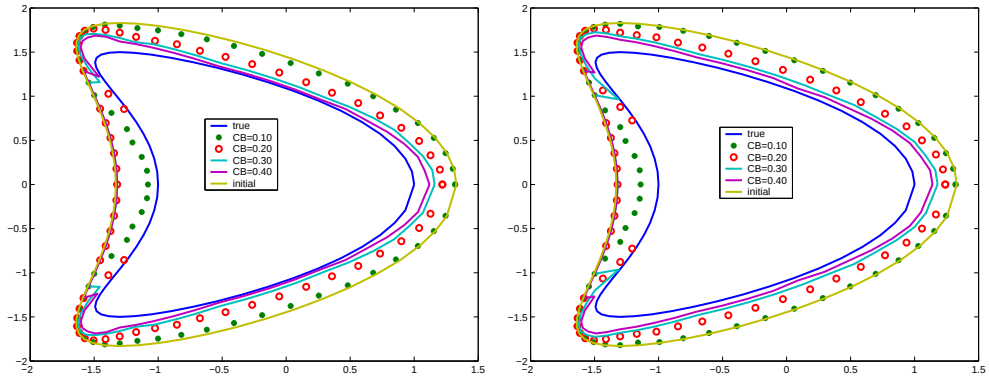

FIG. 5.8. *Reconstruction for the surface impedance relating to the curvature: $f''(x) + \kappa\sigma^i(x) \equiv -5$ (left) and $f''(x) + \kappa\sigma^i(x) \equiv -10$ (right). The introduction of the variable imaginary part of surface impedance in terms of the curvature distribution removes the nonuniform blowing up phenomena due to the curvature distribution.*

part of surface impedance is introduced. We also take $\sigma(x) = 5 + \sigma^i(x)i$. The reconstructions with $\sigma^i(x)$ satisfying $f''(x)+\kappa\sigma^i(x) \equiv -5$ (left) and $f''(x)+\kappa\sigma^i(x) \equiv -10$ (right) in ∂D are shown below.

Comparing the two pictures in Figure 5.8, it can be seen that the uniform blowing-up property is obtained, except on the parts near the point E, where the curvature takes the negative minimum value. This phenomena is physically reasonable, since the obstacle near the point E is like a basin. There are multiple reflections of the scattered wave. Due to this multiple reflection and the energy absorbing of the real part of surface impedance, the information about this concave side is relatively small in the far-field data. Therefore, this part can not be improved too much. To explain more about this phenomenon, a higher asymptotic expansion using higher multipole sources is needed. This will be done in a forthcoming work.

Acknowledgement. The first author is supported by NSFC(10771033) and thanks Johann Radon Institute for Computational and Applied Mathematics for its support and hospitality during his stay there. The second author is supported by FWF of the Austrian Academy of Sciences through the project SFB F1308.

REFERENCES

[1] H. Ammari, H. Kang, *Reconstruction of Small Inhomogeneities from Boundary Measurements*, Lecture Notes in Mathematics, Vol.1846, Springer-Verlag, Berlin, 2004.

[2] H. Ammari, E. Iakovleva, S. Moskow, *Recovery of small inhomogeneities from the scattering amplitude at a fixed energy*, SIAM J. Appl. Math., Vol.34, No.4, 882-900.

[3] H. Ammari, E. Iakovleva, D. Lesselier, G. Perrusson, *MUSIC-type electromagnetic imaging of a collection of small three-dimensional inclusions*, SIAM Sci. Comput., Vol.29, (2007), 674-709.

[4] J. L. Buchanan, R. P. Gilbert, A. Wirgin, Y. S. Xu, *Marine acoustics. Direct and inverse problems. Society for Industrial and Applied Mathematics,* Philadelphia, PA, 2004.

[5] F. Cakoni, D. Colton, *The determination of the surface impedance of a partially coated obstacle from far field data*, SIAM. J. Appl. Math., Vol.64, (2004), 709-723.

[6] F. Cakoni, D. Colton, P. Monk, *The determination of the surface conductivity of a partially coated dielectric*, SIAM. J. Appl. Math., Vol.65, No.3, (2005), 767-789.

[7] F. Cakoni, D. Colton, *Qualitative Methods in Inverse Scattering Theory*, Interaction of Mechanics and Mathematics, Springer, 2006.

[8] J. Cheng, J.J. Liu, G. Nakamura, *The numerical realization of the probe method for the inverse scattering problems from the near field data*, Inverse Problems, Vol.21, No.3, (2005), 839-855.

[9] D. Colton, A. Kirsch, *A simple method for solving inverse scattering problems in the resonance region*, Inverse Problems, Vol.12, (1996), 383-393.

[10] D. Colton, R. Kress, *Inverse Acoustic and Electromagnetic Scattering Theory*, 2nd edition, Berlin-Springer, 1998.

[11] A. J. Devaney, *Super resoltion processing of multi-static data usnig time reversal and MUSIC*, Journal of the Acoustical Society of America, to appear.

[12] A. Friedman, M. Vogelius, *Identification of small inhomogeneities of extreme conductivities by boundary mesurements. A theorem on continuous dependence*, Arch. Rat. Mec. Anal. 105 (1989), 299-326.

[13] E. K. Gruber, E. A. Marengo, A. J. Devaney, *Time-reversal imaging with multiple signal classification considering multiple scattering between the targets*, Journal of the Acoustical Society of America, Vol.115, (2004), 3042-3047.

[14] D.J. Hoppe and Y. Rahmat-Samii, *Impedance boundary condition in electromagnetism*, Taylor and Francis, 1995.

[15] N. Honda, G. Nakamura, R. Potthast and M. Sini, *The no-response approach and its relation to non-iterative methods for the inverse scattering*, Ann. Mat. Pura Appl. Vol 187, No.1, (2008), 7–37.

[16] M. Ikehata, *Reconstruction of obstacles from boundary measurements*, Wave Motion, Vol.3, (1999), 205-223.

[17] V. Isakov, *Inverse Problems for Partial Differential Equations*, Springer Series in Applied Math. Science, Berlin: Springer, 127, 2nd edition, (2006).
[18] E. Kerbrat, C. Prada, M. Fink, *Imaging in the presence of gain noise using the decomposition of the time reversal operator*, Journal of the Acoustical Society of America, Vol.113, No.3, (2003), 1230-1240.
[19] A. Kirsch, *Characterization of the shape of a scattering obstacle using the spectral data of the far field operator*, Inverse Problems, Vol.14, (1998), 1489-1512.
[20] E. Klaus, R. Potthast, *A numerical study of the probe method*, SIAM J. Sci. Comput., Vol.28, No.5, (2006), 1597-1612.
[21] R. Kress, *Linear Integral Equations*, Springer-Verlag, Berlin, 1989.
[22] J.J. Liu, G. Nakamura, M. Sini, *Reconstruction of the shape and surface impedance from acoustic scattering data for an arbitrary cylinder*, SIAM J. Appl. Math. Vol.67, No.4, (2007), 1124-1146.
[23] J.J. Liu, M. Sini, *How to make an obstacle more (or less) visible from exterior measurements*, Preprint at RICAM.
[24] G. Nakamura, M. Sini, *Obstacle and boundary determination from scattering data.* SIAM J. Math. Anal, V:39, N: 3 p:819-837.
[25] G. Nakamura, R. Potthast, M. Sini, *Unification of the probe and singular sources methods for the inverse boundary value problem by the non-responce test*, Comm. PDE, Vol.31, No.10, (2006), 1505-1528.
[26] R. Potthast, *Point Sources and Multipoles in Inverse Scattering Theory*, Research Notes in Mathematics, Vol.427, Chapman-Hall/CRC, Boca Raton, Fl, 2001.
[27] R. Potthast, *Sampling and probe methods - an algorithmical view*, Computing, Vol.75, No.2-3, (2005), 215–235.
[28] R. Potthast, *A survey on sampling and probe methods for inverse problems*, Inverse Problems, Vol.22, No.2, (2006), R1-R47.
[29] C. Prada, J. L. Thomas, *Experimental subwavelenght localization of scattering bs decomposition of the time reversal operator interpreted as a covariance matrix*, Journal of the Acoustical Society of America, Vol.114, No.1, (2003), 235-243.
[30] A. Ramm, *Wave Scattering by small bodies of arbitrary shapes*, World Scientific Publisher, 2005.
[31] R. O. Schmidt, *Multiple emitter location and signal parameter estimation*, IEEE Trans. Antennas Propagation, Vol.34, No.3, (1986), 276-280.